This article has been accepted for publication in a future issue of this journal, but has not been fully edited. Content may change prior to final publication. Citation information: DOI 10.1109/JESTPE.2018.2868950, IEEE Journal of Emerging and Selected Topics in Power Electronics

An electrolytic capacitorless modular three-phase ac-dc LED driver based on summing the light output of each phase

Ignacio Castro, *Member, IEEE*, Aitor Vazquez, *Member, IEEE,* Diego G. Lamar, *Member, IEEE,* Manuel Arias, *Member, IEEE*, Marta M. Hernando, *Senior Member, IEEE* and Javier Sebastian*, Senior Member, IEEE*.

Departamento de Ingeniería Eléctrica, Electrónica, de Computadores y Sistemas, Gijón 33204, Spain
(e-mail: gams.castro@gmail.com)

Abstract— The proposal of this work is a modular three-phase ac-dc LED driver for high power luminaires based on Light-Emitting Diodes (LEDs), that uses each phase to control an independent LED load removing in the process both the electrolytic capacitor and the second stage to increase both the lifetime and the efficiency. The driving of each LED load is done by means of a dc-dc converter operating as a Loss Free Resistor responsible for controlling the current across it. Furthermore, each dc-dc converter needs to achieve Power Factor Correction (PFC) to comply with the restrictive IEC 61000-3-2 Class C requirements. Hence, achieving unity Power Factor (PF) and low Total Harmonic Distortion (THD). Taking advantage of the light properties, the output of the LED driver will be the sum of the light of each of the phases. Therefore, a theoretical study will be carried out to observe the feasibility of removing the electrolytic capacitor while guaranteeing a flicker free behaviour of the LED luminaire, even if the current of each string is pulsating at twice the mains frequency. This particular performance under high output current and voltage ripples requires reevaluating the well-known limits between the conduction modes in PFC converters. In addition, the theoretical analysis also discusses and proposes control methods for the LED driver, which thanks to its modularity can easily scale in power to drive high power luminaires.

In order to validate the theoretical analysis, a prototype has been built comprised of three PFC boost converters disposing of their electrolytic capacitors. The designed prototype operates in the full range of the European three-phase line voltage, which varies between 380 V and 420 V, and supplies an output light of 42.000 lm at a maximum power of 300 W while achieving an electrical efficiency of 97.5%.

Keywords— Single phase, ac-dc power conversion, Power Factor Correction, HB-LED driver

I. INTRODUCTION

Light-Emitting Diodes (LEDs) are becoming increasingly ubiquitous across all aspects of illumination products due to their reliability, long lifetime, energy efficiency and low maintenance requirements. These advantages make LEDs suitable to replace traditional lamps in household, commercial and industrial installations [1]. Specifically, this work focuses in replacing high power lamps, i.e. 200 W to 10 kW, at almost inaccessible locations, such as tunnel lights, stadium spotlights or floodlights, where access to the three-phase power grid is also available.

Conventionally, single-phase LED drivers need to comply with both ENERGY STAR® [2], [3] and the harmonic injection regulation IEC 61000-3-2 [4]. The first requires the driver to achieve a Power Factor (PF) of 0.9 and a lifetime of more than 50,000 h in commercial environments. In fact, the lifetime is considered as the elapsed operating time over which the LED light source will maintain a 70% of its initial light output. The compliance with the lifetime requirement makes mandatory the disposal of the electrolytic capacitor from ac-dc LED drivers, which has been a major research topic in ac-dc LED drivers. This feat has been performed in single-phase with the addition of a bidirectional converter [5], [6], a partially cascaded dc-dc converter [7], [8] or a fully cascaded dc-dc converter [1] that in some cases can be integrated within the PFC converter [9], [10]. However, this is not the case for three-phase ac-dc LED drivers as they can perform the disposal of the electrolytic capacitor naturally.

The harmonic injection regulation IEC 61000-3-2 requires the driver to comply with Class C for lamps of more than 25W. In fact, for three-phase LED drivers the regulation is not clear since the driver falls into Class A category according to it being balanced three-phase equipment, or into Class C because it is also lighting equipment. The aim of this work will be complying with the most restrictive regulation, which is Class C. In that case, each phase of the driver will be required to demand a sinusoidal current in phase with its phase voltage.

Considering that an LED driver needs to be cheap and reliable, a three-phase single-switch converter will be ideal. In fact, a single-switch three-phase flyback converter [11], [12] has been previously proposed to drive LEDs, as illustrated in Fig. 1 (a). However, its PF is roughly 0.9 for the higher voltages of the European three-phase grid, its efficiency is well below the desired 90% for an LED driver and the switch needs

This work was supported in part by the Spanish Government under Project MINECO-17-DPI2016-75760-R, in part by the Principality of Asturias under Severo Ochoa grant BP14-142, Project FC-15-GRUPIN14-143 and Project SVPA-17-RIS3-4, and in part by European Regional Development Fund (ERDF) grants.

This article has been accepted for publication in a future issue of this journal, but has not been fully edited. Content may change prior to final publication. Citation information: DOI 10.1109/JESTPE.2018.2868950, IEEE Journal of Emerging and Selected Topics in Power Electronics

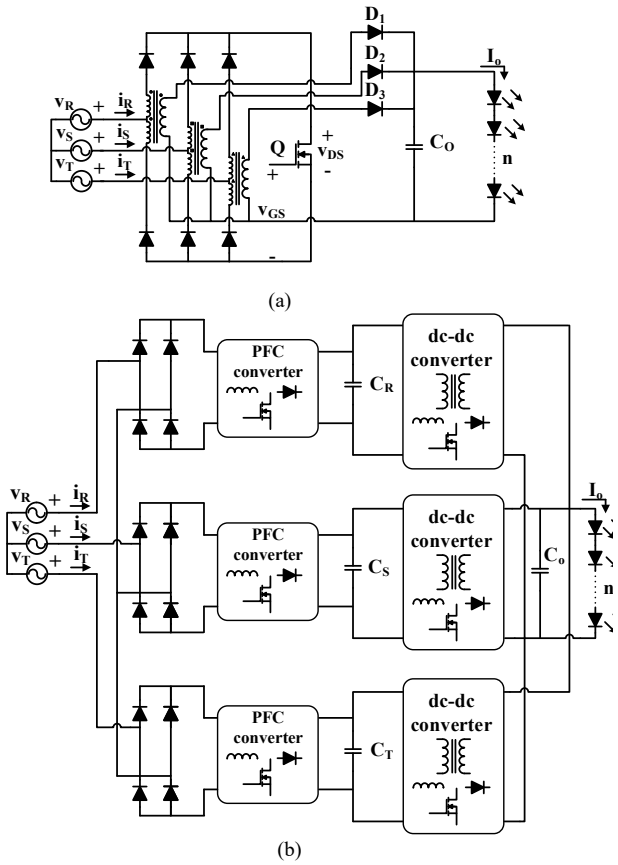

Fig. 1. Isolated three-phase rectifier. (a) Single-switch three-phase ac-dc flyback LED driver. (b) Multicell three-phase ac-dc LED driver based on using three single phase converters with fictional neutral connection.

to withstand high voltages unless a snubber is used [13]. These characteristic make this driver unfitting for luminaries of more than 200 W.

In accordance to previous literature, another feasible LED driver for this application is based on a modular approach and is able to comply with the aforementioned regulation, either with three cells [14], [15], or six cells to achieve higher efficiencies [15]-[17]. The proposal of these works to drive LED luminaires is to use a cell based on either a single-stage or a two-stage approach per phase, as illustrated in Fig. 1 (b). The latter being used for high power luminaires due to the limitations of single-stage isolated solutions. In the second scenario, each cell is comprised of a first stage that achieves Power Factor Correction (PFC), typically a boost converter, followed by a fixed-gain isolated step-down dc-dc converter to adjust voltages and currents to that of the LED string [18]. In fact, this approach is similar to the two-stage single-phase ac-dc solution, and the second stage can be implemented by means of resonant converters [19], as an Asymmetrical Half-Bridge (AHB) [20] or a Zeta AHB [21].

The galvanic isolation of the second stage is required in this LED driver to be able to connect the outputs of each cell in parallel to the LEDs, as shown in Fig. 1 (b). The parallel connection is necessary to eliminate the electrolytic capacitor, otherwise present in single-stage ac-dc converters if the second stage does not have the proper control. However, this solution requires an excessive amount of components, which would hinder its reliability and penalize the efficiency of the LED driver at lower loads due to the second stage. In fact, taking into account the aim of this work for low maintenance LED lamps placed in inaccessible locations galvanic isolation can be removed, as only authorized personnel should have access to the LED lamp and driver.

Some authors have tackled the design of three-phase non-isolated LED drivers based on switched capacitors [22]. These drivers can achieve high power density, high efficiency and do not require current sensing to maintain a stable light output. In contrast, the proposal requires variable frequency operation, cannot achieve full dimming condition and requires six active switches, which similarly to the multi-cell approach, previously described, will hinder the reliability of the driver.

In order to solve the reliability and cost issues, the proposal of this work is based on eliminating the isolated dc-dc converter that comprises the multi-cell approach, depicted in Fig. 1 (b). Hence, directly connecting an LED string to each PFC converter, as shown in Fig. 2. It should be noted that, any PFC converter as long as it operates as a Loss Free Resistor (LFR) is able to perform this achievement. This statement increases the amount of potential topologies that can be used as cells of the proposed topology, taking into account galvanic isolation is no longer a mandatory condition. Thus, a boost converter operating as a PFC can be used with High Voltage (HV) LEDs. The HV LED driving approach has been studied by a handful of authors thanks to the newer LEDs recently introduced in the market, showing promising results to reduce cost and increase the reliability of drivers [23].

The main benefit that all previous three-phase LED drivers share is the removal of the most limiting component in terms of lifetime, which is the electrolytic capacitor. This is achieved due to the non-pulsating power at the load in a balanced three-phase power grid. However, in the proposed LED driver, the size of the output capacitor of each cell (i.e. C_R, C_S and C_T,

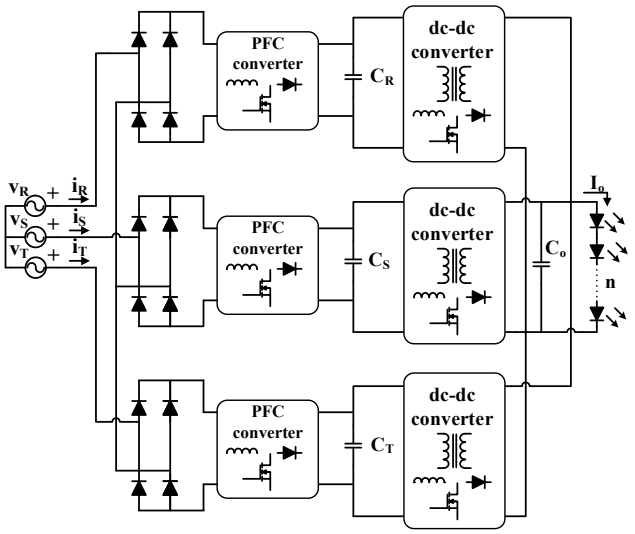

Fig. 2. Proposed LED driver based on a modular approach without galvanic isolation.

This article has been accepted for publication in a future issue of this journal, but has not been fully edited. Content may change prior to final publication. Citation information: DOI 10.1109/JESTPE.2018.2868950, IEEE Journal of Emerging and Selected Topics in Power Electronics

referred as C_X) cannot be diminished, if a constant current is to be assured to drive each string.

In order to comply with the lifetime requirements of ENERGY STAR®, this work analyzes the reduction of C_X, allowing a certain ripple to appear in terms of the current across the LEDs. This ripple will modulate the amplitude of the light due to the well-known relationship between current and light on an LED [24], hence, causing a perceptible flicker on each phase. It should be noted that, this current modulation of a low frequency ac signal plus a dc signal does not have any impact in terms of the lifetime of the LEDs [25]. In contrast, the perceptible flicker both annoying and hazardous for human beings is not an issue for this solution, considering that the low frequency modulation of the light is cancelled between phases, rendering a constant light output [26].

Therefore, the aim of this work is proposing a three-phase multi-cell ac-dc LED driver capable of achieving high efficiencies to drive high power luminaires based on LED loads, while still keeping the design of the cell as simple as possible, and without using an electrolytic capacitor. For that matter, Section II studies the feasibility of removing the electrolytic capacitor in the proposed solution by means of an analytical study. In fact, considering the potentially high variation of the output voltage allowed with the usage of low output capacitances compared to the conventional approach, it is also necessary to study the limits of operation between Continuous Conduction Mode (CCM) and Discontinuous Conduction Mode (DCM), carried out in Section III and particularized for the boost PFC converter. Section IV is dedicated to the proposed control methods for the LED driver under study, carefully stating the required start-up and proposing two methods of controlling the LED driver. Section V focuses on the experimental results obtained with three PFC boosts working as cells, each handling a maximum power of 100 W. This results lead to the discussion of the conclusions extracted from this work in Section VI.

II. Working Principle

The proposed driver takes advantage of the sum of the light output of each cell to guarantee a flicker free behaviour while disposing of the second stage required in a multi-cell three-phase LED driver. Understanding the operation of a dc-dc converter as an LFR is key to guarantee compliance with the harmonic regulation, removal of the electrolytic capacitor and the ability to achieve full dimming. An LFR performance is available for converters from the family of either boost or buck-boost, either by operating in CCM with a Multiplier Based Control (MBC) [27], in Boundary Conduction Mode (BCM) [28] or with a Voltage Follower Control (VFC) [29]. This operation guarantees a resistor behaviour at its input by shaping the input current in accordance to its input voltage, and whose value, R_{LFR}, depends on a control variable. The output performance is that of an ideal power source that depends on the demanded input power. In fact, by considering the PFC converters as an ideal LFR, Fig. 2 can be redrawn as Fig. 3, where the LEDs are replaced with their equivalent circuit comprised of: an ideal diode, an equivalent dynamic resistance

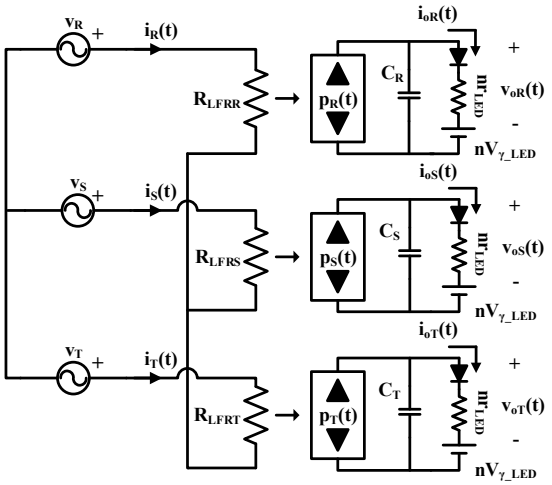

Fig. 3. Equivalent LFR model of the proposed LED driver based on a modular approach without galvanic isolation.

(r_{LED}) and an ideal voltage source, representing the knee voltage of the diode (V_{γ_LED}). The circuital problem is then reduced to a star network of equal resistors (i.e. $R_{LFRR}=R_{LFRS}=R_{LFRT}$) at the input, and an ideal power source feeding both the output capacitor and a string of LEDs at the output of each cell.

The first study carried out is to estimate the theoretical ripple of the low frequency component that modulates the output luminance of the driver (l_o) without an output capacitor. Then, the study will be completed using an output capacitor of equal value on each cell.

In order to calculate $l_o(t)$, the currents through the LEDs, $i_{oR}(t)$, $i_{oS}(t)$ and $i_{oT}(t)$, need to be determined. In addition, considering the sum of these currents to be proportional to the light supplied by the LEDs, then,

$$l_o(t)=\alpha\left(i_{oR}(t)+i_{oS}(t)+i_{oT}(t)\right), \tag{1}$$

where α represents the proportionality between the low frequency modulation of the light and the current through the LEDs.

A. Without output capacitor

This first study will shed some light on whether it is feasible to achieve a non-flicker performance when driving the LEDs with pulsating currents. The current through the LEDs can be obtained by analyzing and solving a simple circuit of a power source in parallel with the LEDs, taking into consideration that capacitance C_R, C_S and C_T from Fig. 3 are removed for this analysis. Hence,

$$p_X(t)=i_{oX}^2(t)nr_{LED}+i_{oX}(t)nV_{\gamma\_LED}, \tag{2}$$

where n represents the amount of LEDs in series in an LED string and X represents the phase under study, R, S or T which are given a fixed value to unify and simplify the analysis. Consequently, X is equal to 0 for phase R, 1 for phase S and 2 for phase T. Then, solving for i_{oX} in (2), yields,

This article has been accepted for publication in a future issue of this journal, but has not been fully edited. Content may change prior to final publication. Citation information: DOI 10.1109/JESTPE.2018.2868950, IEEE Journal of Emerging and Selected Topics in Power Electronics

$$i_{oX}(t)=\frac{-nV_{\gamma\_LED}+\sqrt{n^2V_{\gamma\_LED}^2+4nr_{LED}p_X(t)}}{2nr_{LED}}, \quad (3)$$

where,

$$p_X(t)=I_gV_g\sin^2\left(\omega t-X\frac{2\pi}{3}\right), \quad (4)$$

V_g and I_g are the mains peak input voltage and current, respectively, and ω is the mains angular frequency.

By operating with (1) and (3), the output luminance can be obtained. However, this is not a practical expression and conclusions cannot be easily drawn from it, unless it is processed with a numerical computing environment. For that matter and considering that this is a periodic waveform, the Fourier series can be applied marking the 60th harmonic as the limit in accordance to the flicker regulation. However, this is a difficult Fourier series to determine, so the Fourier series is attained by means of graphical characterization considering that commercially available LEDs present low values of r_{LED}. The theoretical waveform has been represented, studied and compared with two approximations in both time and frequency domain, as illustrated in Fig. 4. The first one is based on the traditional current waveform at the output of a PFC converter with unity PF, which does not present a component at six times the line frequency. Thus, the Fourier series approximation is proposed:

$$l_o(t)=\frac{L_{max}+L_{min}}{2}-\frac{L_{max}-L_{min}}{2}\cos(6\omega t), \quad (5)$$

where,

$$L_{min}=\alpha\frac{-nV_{\gamma\_LED}+\sqrt{n^2V_{\gamma\_LED}^2+3nr_{LED}P_g}}{nr_{LED}}, \quad (6)$$

and

$$L_{max}=\alpha\frac{-nV_{\gamma\_LED}+\sqrt{n^2V_{\gamma\_LED}^2+4nr_{LED}P_g}}{2nr_{LED}}+\alpha\frac{-nV_{\gamma\_LED}+\sqrt{n^2V_{\gamma\_LED}^2+nr_{LED}P_g}}{nr_{LED}}, \quad (7)$$

are the maximum and minimum luminance of the LED luminaire, obtained from combining (1) and (3) and solving at $\omega t = 0$ and $\omega t = \pi/2$, respectively, and P_g is the peak input power (i.e. $P_g = V_gI_g$) of one of the phases, considering that ideally all the phases demand the same amount of power.

In (5), it can be seen that the output luminance is comprised of a dc and a sinusoidal component of six times the line frequency. If r_{LED} is considered to be negligible, then (6) and (7) can be approximated by,

$$L_{min}(r_{LED}=0)=L_{max}(r_{LED}=0)=\frac{3\alpha P_g}{2nV_{\gamma\_LED}}. \quad (8)$$

Eq. (8) is obtained after solving the zero divided by zero indetermination that appears from substituting $r_{LED} = 0$ in both (6) and (7).

It should be noted that the deviation that occurs between L_{min} and L_{max} becomes remarkable for high values of r_{LED} (i.e. > 100 Ω). However, the available LEDs on the market do not present such high values of r_{LED}. Hence, $l_o(t)$ can be approximated to be a constant value close to either L_{max} or L_{min}, not showing any flicker on the light output under ideal conditions.

This analysis is able to validate the removal of the output capacitor. However, even if this operation is desirable in terms of light output, it is not from the perspective of the current supplied to each LED string due to the high current ripple withstood. This will require the LEDs to be oversized or even increase the amount required to ensure a safe operation in terms of their maximum current rating, not in terms of the average current across them. Therefore, a study needs to be carried out to evaluate the adequate size of the output capacitor in terms of the output current ripple, to adjust the current levels while still using a film or ceramic capacitor that has an acceptable lifespan to comply with ENERGY STAR®.

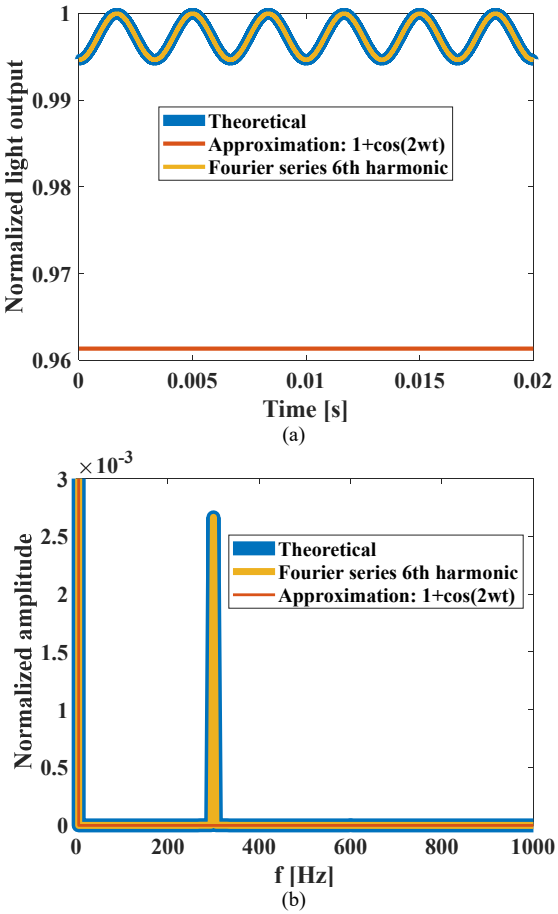

Fig. 4. Graphical characterization of the Fourier series for the proposed converter. (a) Time domain. (b) Frequency domain.

This article has been accepted for publication in a future issue of this journal, but has not been fully edited. Content may change prior to final publication. Citation information: DOI 10.1109/JESTPE.2018.2868950, IEEE Journal of Emerging and Selected Topics in Power Electronics

B. With output capacitor

The addition of an output capacitor requires to start over the mathematical analysis previously carried out. For that reason, (2) can be rewritten as,

$$p_X(t)=C_X v_{oX}(t)\frac{dv_{oX}(t)}{dt}+v_{oX}(t)i_{oX}(t), \quad (9)$$

where $v_{oX}(t)$ can be defined as,

$$v_{oX}(t)=nV_{\gamma\_LED}+i_{oX}(t)nr_{LED}. \quad (10)$$

and where C_X defines the capacitance of the output capacitor of one of the cells that comprise the LED driver, as seen in Fig. 2. Eq. (9) is a complex differential equation that requires knowing beforehand the mathematical expression of the solution. Fortunately, it is well-known that the output current ($i_{oX}(t)$) should follow the expression of a sinusoidal waveform at twice the line frequency with a certain dc level, taking into account the voltage source behavior of the LEDs. Hence,

$$i_{oX}(t)=I_{ac}\sin\left(2\omega t-\varphi-\frac{2\pi}{3}X\right)+I_{dc}, \quad (11)$$

where I_{ac} is the peak value of the ac component, I_{dc} is the dc level of the output current and φ represents a phase delay. Substituting (11) into (9), is the start point of this mathematical analysis in order to attain the three aforementioned parameters (i.e. I_{ac}, I_{dc} and φ). The study for phase R yields,

$$P_g\sin^2(\omega t)=A_1 I_{ac}\cos(2\omega t-\varphi)+A_2 I_{ac}\sin(2\omega t-\varphi)+\left(\frac{I_{ac}^2}{2}+I_{dc}^2\right)nr_{LED}+I_{dc}nV_{\gamma\_LED}, \quad (12)$$

if the four times the line frequency components are removed and losses are not considered, where A_1 and A_2 are defined as,

$$A_1=C_X nr_{LED}\left(nr_{LED}I_{dc}+nV_{\gamma\_LED}\right)2\omega, \quad (13)$$

$$A_2=\left(2nr_{LED}I_{dc}+nV_{\gamma\_LED}\right). \quad (14)$$

Grouping components in (12) in terms of the dc and sinusoidal components of double the line frequency renders,

$$\frac{P_g}{2}=\left(\frac{I_{ac}^2}{2}+I_{dc}^2\right)nr_{LED}+I_{dc}nV_{\gamma\_LED}, \quad (15)$$

and

$$\frac{-P_g}{2}\cos(2\omega t)=A_1 I_{ac}\cos(2\omega t-\varphi)+A_2 I_{ac}\sin(2\omega t-\varphi). \quad (16)$$

Looking at (15) and (16), it can be seen that both equations are dependent of I_{ac} and I_{dc} which gives a system of two equations and three unknown variables. In order to attain a useful model from an engineering perspective, there is one simplification that can be performed, which is removing I_{ac} from (15). This approximation dramatically decreases the complexity of the solutions, and can be performed due to two reasons:

1. An LED load is used at the output of each cell. Thus, the impact of the ac component on the total losses in comparison to the dc component can be considered negligible since it only multiplies the dynamic resistance, which has a much lower value than the knee-voltage of the LED.
2. The maximum achievable value of I_{ac} is equal to I_{dc} if no capacitor is used on the cells. In fact, the higher the value of the output capacitance the lower the value of I_{ac} due to the diminishment of the output current ripple of the cell.

For these two reasons, I_{ac} is removed, achieving an error of less than 5% without output capacitance, which gets lower the higher the value of the output capacitance is. Now, I_{dc} can be easily obtained by solving (15) without the I_{ac} terms as,

$$I_{dc}=\frac{-nV_{\gamma\_LED}+\sqrt{n^2V_{\gamma\_LED}^2+2nr_{LED}P_g}}{2nr_{LED}}. \quad (17)$$

In order to attain I_{ac} and φ, it is necessary to solve (16). This equation can be simply solved by applying wave superposition theory, which is widely used in other fields of study [30], reducing the problem to the sum of two plane waves with different amplitude. Hence,

$$I_{ac}=\frac{-P_g}{2\sqrt{A_1^2+A_2^2}}, \quad (18)$$

$$\varphi=\tan^{-1}\left(\frac{-A_2}{A_1}\right). \quad (19)$$

Having calculated all the parameters, a relationship between the required output capacitance for a certain peak-to-peak current ripple (ΔI) can be made from (18). The first step is to substitute (13) into (18), obtaining:

$$I_{ac}=\frac{-P_g}{2\sqrt{\left(C_X nr_{LED}\left(nr_{LED}I_{dc}+nV_{\gamma\_LED}\right)2\omega\right)^2+A_2^2}}. \quad (20)$$

Then, (20) is squared and terms are grouped to help solving for C_X, yielding,

$$\left(I_{ac}^2 4C_X nr_{LED}\left(nr_{LED}I_{dc}+nV_{\gamma\_LED}\right)2\omega\right)^2=P_g^2-I_{ac}^2 4A_2^2. \quad (21)$$

Now, it is possible to solve for C_X in (21), giving the next expression:

$$C_X=\frac{1}{I_{ac}^2 4nr_{LED}\left(nr_{LED}I_{dc}+nV_{\gamma\_LED}\right)2\omega}\sqrt{P_g^2-I_{ac}^2 4A_2^2}, \quad (22)$$

By operating with (21) the next relationship can be yielded,

$$C_X=\frac{1}{nr_{LED}\left(nr_{LED}I_{dc}+nV_{\gamma\_LED}\right)2\omega}\sqrt{\frac{P_g^2}{4I_{dc}^2\Delta I^2}-A_2^2}. \quad (23)$$

This article has been accepted for publication in a future issue of this journal, but has not been fully edited. Content may change prior to final publication. Citation information: DOI 10.1109/JESTPE.2018.2868950, IEEE Journal of Emerging and Selected Topics in Power Electronics

considering that I_{ac} can be defined as I_{dc} multiplied by ΔI.

At this point, it becomes necessary to normalize the previous equations in order to attain a useful model. For that matter, solving (13), (14) and (15) into (18), considering the approximation previously taken into account for (15), yields,

$$I_{ac,norm}I_{dc}=\frac{-I_{dc}(I_n+1)}{\sqrt{(2I_n+1)^2+k_n^2(I_n+1)^2}}, \tag{24}$$

where,

$$k_n=2\omega C_X n r_{LED}, \tag{25}$$

$$I_n=\frac{I_{dc}}{V_{\gamma\_LED}/r_{LED}}. \tag{26}$$

Similarly, solving (13), (14) and (15) into (19), gives,

$$\varphi_{norm}=\tan^{-1}\left(\frac{-(2I_n+1)}{k_n(I_n+1)}\right). \tag{27}$$

From here, it is now possible to solve (24) and (27) into (11), and then factorize in terms of I_{dc}, obtaining,

$$i_{oX,norm}(t)=I_{dc}\left[I_{ac,norm}\sin\left(2\omega t-\varphi-\frac{2\pi}{3}X\right)+1\right]. \tag{28}$$

Eq. (28) depends on I_{dc}, t and $I_{ac,norm}$, which at the same time depends on k_n and I_n. Hence, it is possible to study the impact of the variation of k_n, which varies linearly with the output capacitance, and I_n, which is a parameter heavily reliant on LED technology and whose value tends to be minimized with the newer LEDs, on the output current for a certain I_{dc}. For that matter, Fig. 5 (a) and (b) show the normalized output current when varying the aforementioned parameters. As can be seen, the output current ripple increases as k_n decreases, which means that the ripple increases as the output capacitance decreases, and that I_n does not have an impact on the analysis, considering the lower I_n used as a feasible value for the newer LEDs and the higher as an unreachable limit considering the current LED technology. In summary, this analysis shows that it is possible to diminish the ripple to a certain extent without using an electrolytic capacitor; likewise, it is necessary to foresee under this conditions whether it is possible or not to obtain a constant dc light output.

Substituting (11) into (1), gives the light output waveform of the proposed converter with an output capacitor in each cell, as

$$\begin{aligned} l_o(t)=\alpha\big(&I_{ac}\sin(2\omega t-\varphi)+I_{dc}+I_{ac}\sin\left(2\omega t-\varphi-\frac{2\pi}{3}\right)\\ &+I_{dc}+I_{ac}\sin\left(2\omega t-\varphi-\frac{4\pi}{3}\right)+I_{dc}\big)=\alpha 3I_{dc}, \end{aligned} \tag{29}$$

taking into account that the sinusoidal components cancel each other. Hence, it is feasible to attain a constant light output with a non-electrolytic capacitor that is also able to reduce the current ripple to acceptable levels.

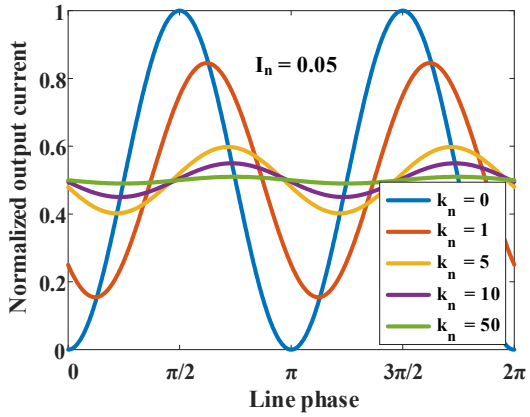

(a)

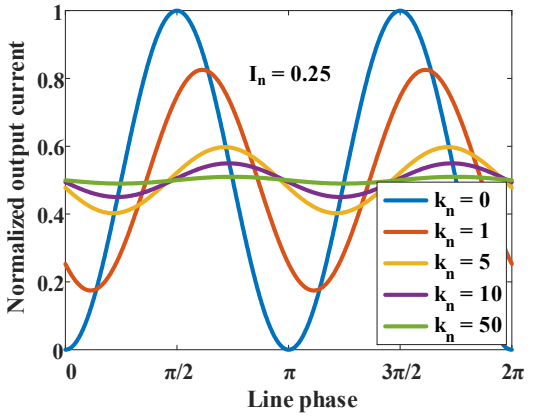

(b)

Fig. 5. Normalized output current versus line phase in terms of k_n for (a) I_n equal to 0.05 and (b) I_n equal to 0.25.

III. Limits between CCM and DCM

The higher ripple allowed at the output of each of the cells, both in voltage and current, does not correspond with the conventional operation of a PFC converter, in which the voltage and current are to be as constant as possible. Under the last assumption, the limits between CCM and DCM have been already studied in [31]. Hence, it is required to study the limits between CCM and DCM under high ripple conditions. In fact, this study proves to be key in order to correctly design and select the magnetic component of the LFR cells. For this reason, the study will include a scenario with fixed switching frequency, and variable switching frequency scenario (i.e. BCM), in which this variation will also be analyzed both in terms of the output capacitance. It should be noted that, this section is particularized for a boost PFC converter, however, following the same criteria it is possible to attain the same expressions for any other converter operating as an LFR.

This article has been accepted for publication in a future issue of this journal, but has not been fully edited. Content may change prior to final publication. Citation information: DOI 10.1109/JESTPE.2018.2868950, IEEE Journal of Emerging and Selected Topics in Power Electronics

A. *Fixed switching frequency*

The first parameter that needs to be calculated is the dc voltage conversion ratio that can be defined by relating the input and output voltage as,

$$m(\omega t)=\frac{nV_{\gamma\_LED}+I_{dc}nr_{LED}}{V_g|\sin(\omega t)|}+\frac{I_{ac}\sin(2\omega t-\varphi)nr_{LED}}{V_g|\sin(\omega t)|}, \quad (30)$$

where the first term represents the conventional component studied in [31] and the second and newer term represents the ripple.

At this point, the analysis requires to obtain the load as it is seen by converter, which is defined by,

$$r(\omega t)=\frac{\left(nV_{\gamma\_LED}+\left(I_{ac}\sin(2\omega t-\varphi)+I_{dc}\right)nr_{LED}\right)^2}{P_g\sin^2(\omega t)}. \quad (31)$$

The limits between CCM and DCM can be studied similarly to any dc-dc converter by obtaining the mathematical expression of $k(\omega t)$ and k_{crit}. $k(\omega t)$ is a well-known parameter specified by,

$$k(\omega t)=\frac{2L}{T_{sw}r(\omega t)}, \quad (32)$$

where T_{sw} is the switching period of the boost converter and L is the input inductance. k_{crit} is the value of $k(\omega t)$ that defines the boundary between CCM and DCM. Hence, if $k(\omega t)$ is greater than k_{crit} the converter will work in CCM, otherwise it will work in DCM. k_{crit} can be determined, according to [30], as,

$$k_{crit}(\omega t)=\frac{m(\omega t)-1}{m(\omega t)^3}. \quad (33)$$

Consequently, it is possible to obtain the limits between modes for the presented conditions. Therefore, for operation in CCM, solving (31) into (32), (30) into (33) and applying that $k(\omega t)$ has to be greater than k_{crit}, renders,

$$\frac{2LP_g}{T_{sw}V_g^2}>\max\{K_1\}, \quad (34)$$

where,

$$K_1(\omega t)=\frac{v_{oX}(t)-V_g|\sin(\omega t)|}{v_{oX}(t)}. \quad (35)$$

Maximizing K_1 in (34) yields the condition that guarantees CCM operation in whole line period, which is defined as,

$$\frac{2LP_g}{T_{sw}V_g^2}>1. \quad (36)$$

Henceforth, it is possible to obtain the inductance value that guarantees CCM operation from (31) as,

$$L>\frac{T_{sw}V_g^2}{2P_g}, \quad (37)$$

In a similar fashion, for operation in DCM,

$$\frac{2LP_g}{T_{sw}V_g^2}<\min\{K_1\}. \quad (38)$$

needs to be satisfied. Unfortunately, the minimization of K_1 to achieve DCM operation for the whole line period is not trivial and the function needs to be numerically solved. For that matter, and in order to alleviate the study, (35) will be normalized, substituting (10) and then (28) into it. Thus, obtaining,

$$K_{1,norm}(\omega t)=1-\frac{V_{gn}|\sin(\omega t)|}{1+I_n\left[\frac{I_{ac,norm}}{I_{dc}}\sin(2\omega t-\varphi)+1\right]}. \quad (39)$$

where,

$$V_{gn}=\frac{V_g}{nV_{\gamma\_LED}}, \quad (40)$$

It is this dependency of K_1 on parameters that at the same time depend on the output capacitance (i.e. I_{ac} and φ), which cause the difficulty of obtaining an analytical solution for its minimization. This fact marks an important difference for a DCM design when compared to the solution obtained in [31]. Consequently concluding the design conditions and selection of the main inductance of each cell, which is of importance for PFC boost in order to diminish THD or for those control techniques that require operation in CCM, such as, one cycle control [32] or voltage ramp compensation control [33], or for a voltage-follower control which would require operation in DCM [34].

B. *Variable switching frequency*

The analysis for BCM focuses on studying the switching frequency limits. For that matter, if an LFR performance is obtained, the input power of the phases can be defined as,

$$p_X(t)=\frac{V_g^2}{L}t_{on}\sin^2\left(\omega t-\frac{2\pi}{3}X\right), \quad (41)$$

where t_{on} defines the constant on time of the main switch. Averaging (38) and solving for t_{on} yields,

$$t_{on}=\frac{P_gL}{V_g^2}. \quad (42)$$

By applying volt-second balance to the inductor, the next expression can be obtained,

$$\frac{V_g|\sin(\omega t)|}{L}t_{on}+\frac{v_{oX}(t)-V_g|\sin(\omega t)|}{L}t_{off}(t)=0, \quad (43)$$

where $t_{off}(t)$ defines the variable off time in the main switch. Solving for $t_{off}(t)$ in (41) and considering the variation of the period over a line cycle, yields,

$$T_{sw}(t)=t_{on}+t_{off}(t)=\frac{v_{oX}(t)t_{on}}{v_{oX}(t)-V_g|\sin(\omega t)|}. \quad (44)$$

This article has been accepted for publication in a future issue of this journal, but has not been fully edited. Content may change prior to final publication. Citation information: DOI 10.1109/JESTPE.2018.2868950, IEEE Journal of Emerging and Selected Topics in Power Electronics

Consequently, the switching frequency (f_{sw}) can be obtained from (44) solving (10) into it, as,

$$f_{sw}(t)=\frac{nV_{\gamma\_LED}+i_{oX}(t)nr_{LED}-V_g|\sin(\omega t)|}{\left(nV_{\gamma\_LED}+i_{oX}(t)nr_{LED}\right)t_{on}}. \quad (45)$$

As with the analysis carried out in the previous section, the maximum value of (45) can be easily determined as,

$$f_{sw,max}=\frac{V_g^2}{P_gL}, \quad (46)$$

but the minimum value has to be studied carefully due to the dependency on the output capacitance. In order to adequately analyze the switching frequency variation, (45) needs to be normalized. In that sense, by solving (27) into (45) and factorizing adequately, (45) can be rewritten as,

$$f_{sw,norm}(t)=\frac{K_{1,norm}(\omega t)n^2V_{\gamma\_LED}^2V_{gn}^2}{P_gL}, \quad (47)$$

Eq. (44) gives all the information required to understand the effect of varying several design parameters on the switching frequency of the converter. In fact, k_n is linearly related to C_X, I_n is related to I_{dc} and V_{gn} is related to V_g, while at the same all of them are in function of the LED characteristics. It is then possible to plot (47) in function of the line phase while varying the three aforementioned parameters, one at a time, obtaining Fig. 6 in order to study their effects. In fact, Fig. 6, serves two purposes, the first one is the analysis of the variation of the switching frequency, and the second one is the study of the minimum value of $K_{1,norm}$, through Fig. 6 (a), (b), (c) and (d), introduced in (39). Fig. 6 (a) and (b) show the variation of the switching frequency with k_n for two different values of I_n. As can be seen, for the lower value of I_n the variation of k_n does not affect the switching frequency other than at the minimum, whereas for the higher values it impacts the whole waveform. This effect can be explained due to the ripple increase of both output voltage and current caused by lowering k_n, which means lowering C_X. For that matter Fig. 6 (c) and (d) studies the variation of I_n for two different values of k_n, showing that the variation of I_n impacts the switching frequency similarly for the lower values of In reaching similar minimum values, however, this fact is not true for the higher values. Hence, it can be concluded that the minimum of K_1 needs to be particularized for a specific design in terms of the selected output capacitance. Finally, Fig. 6 (e) and (f), show that, as expected, the variation of V_{gn} changes both the minimum and maximum values.

IV. Control Techniques

The design criteria of the cell for different operation modes have been discussed in the previous sections ensuring a constant light output. However, the control of the cell has not been presented, and LEDs as many other loads require close loop operation to have an adequate current for their driving in order to provide an acceptable light output.

A. Schemes for closed loop operation

In the particular case of the proposed driver, two control loop schemes that can be of interest are proposed. The first one, depicted in Fig. 7 (a), is based on a conventional approach for a PFC converter controlling the output current instead of the output voltage [27], in which each cell will have its output current controlled by means of an independent Current Control Loop (CCL). The CCL controls the variable v_c, which directly impacts the R_{LFR} value of the cell in order to demand more or less power in accordance to a current reference set by the central control. It should be noted that in each of the cells the LFR performance is ensured by means of an Input Current Controller (ICC) in charge of controlling the switches of the PFC converter to adequately shape the input current.

This proposal is simple, follows a conventional approach and assures that the LEDs are driven with a determined average current level. Consequently, the light output should be guaranteed to be constant in accordance to the prior mathematical analysis. In contrast, it is necessary to filter the low frequency components of the output current, hindering in the process the maximum achievable bandwidth. Furthermore, the current reference value needs to be carefully isolated to be able to provide this information to each cell. This can be extrapolated to the signals that are required for the start-up of the LED driver.

The other scheme, illustrated in Fig. 7 (b), controls the light output of the whole LED driver. This method proposes sensing the light output at a fixed distance by means of a photodiode and a transimpedance amplifier that will convert the light to a determined voltage. Then, this voltage is compared to the light reference to calculate the error, which is processed by the Light Current Loop (LCL). Similarly to the CCL, the LCL generates v_c, which will be send via wireless communications to each of the modules. In that sense, this method is similar to the conventional control used for three-phase modular ac-dc converters with a parallel output connection in which the output voltage is the only variable being controlled and the cells receive v_c to set the power they have to supply to the load [16], [35]. Moreover, this scheme will theoretically have the same potential bandwidth as a dc-dc converter, although limited to 300 Hz due to the tolerances of real components, which will cause a certain ripple at that frequency that is required to be filtered. Even so, the bandwidth is improved in comparison with the previous scheme. The main issue comes from requiring a light sensor at a fixed distance with a wireless communication protocol to transmit the required information to the cells, increasing cost and complexity.

A combination of both schemes can also be evaluated to achieve a better performance than the previous schemes with higher bandwidth and a constant light output. However, the increase of complexity does not justify the aforementioned benefits taking into account that LEDs are a dynamically slow load.

This article has been accepted for publication in a future issue of this journal, but has not been fully edited. Content may change prior to final publication. Citation information: DOI 10.1109/JESTPE.2018.2868950, IEEE Journal of Emerging and Selected Topics in Power Electronics

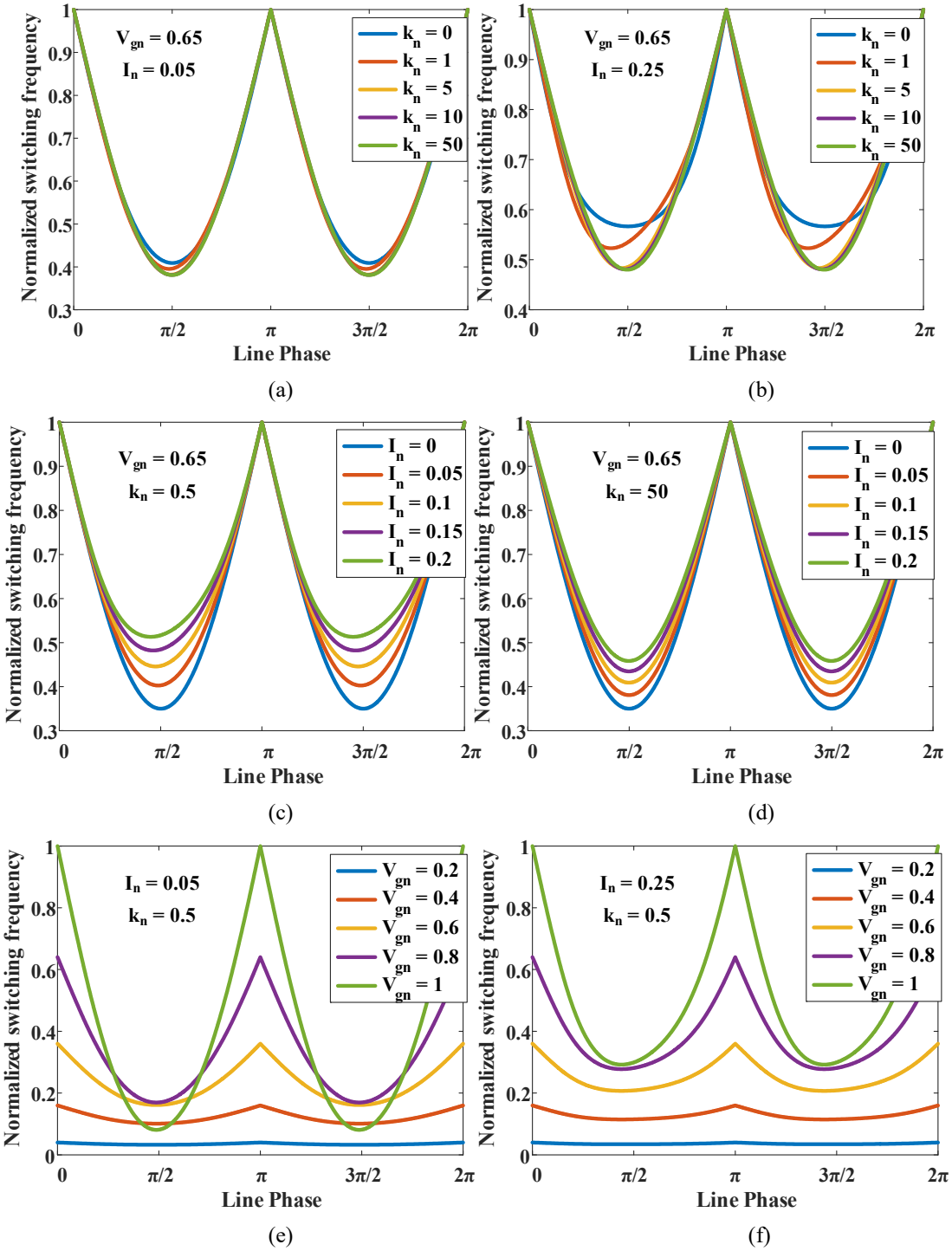

Fig. 6. Normalized switching frequency versus line phase in terms of: (a) k_n for V_{gn} and I_n equal to 0.65 and 0.05, respectively, (b) k_n for V_{gn} and I_n equal to 0.65 and 0.25, respectively, (c) I_n for V_{gn} and k_n equal to 0.65 and 0.5, respectively, (d) I_n for V_{gn} and k_n equal to 0.65 and 50, respectively, (e) V_{gn} for k_n and I_n equal to 0.5 and 0.05, respectively, and (f) V_{gn} for k_n and I_n equal to 0.5 and 0.25, respectively.

This article has been accepted for publication in a future issue of this journal, but has not been fully edited. Content may change prior to final publication. Citation information: DOI 10.1109/JESTPE.2018.2868950, IEEE Journal of Emerging and Selected Topics in Power Electronics

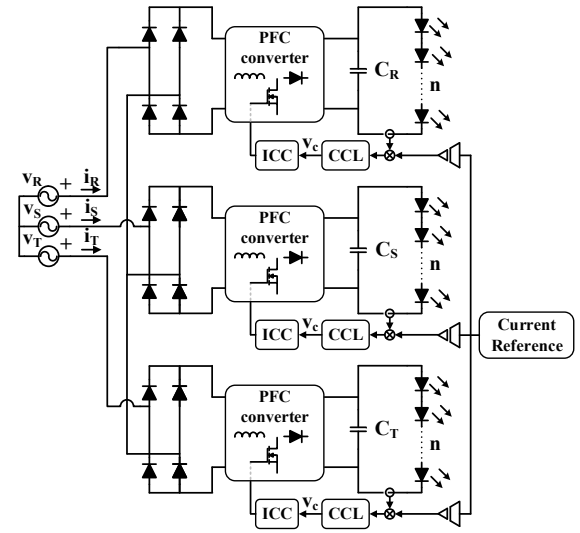

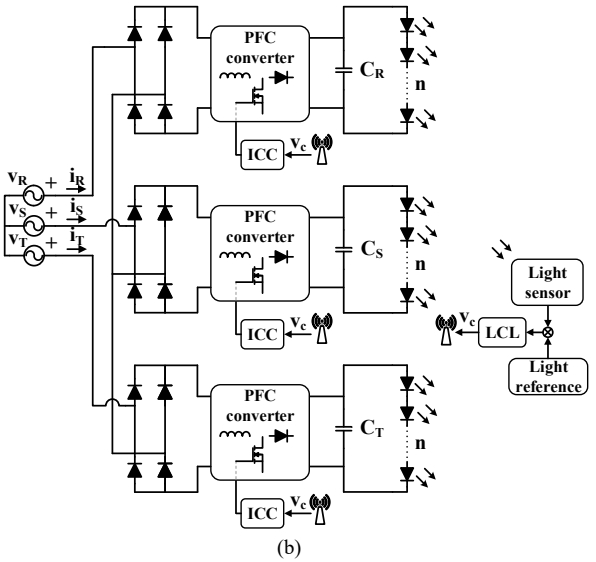

Fig. 7. Closed loop operation. (a) Current closed loop per cell. (b) Light output closed loop operation per LED driver.

B. Average small-signal analysis

In order to design for either of the two presented schemes, it is necessary to obtain a transfer function to control. Firstly, R_{LFR} needs to be defined,

$$R_{LFR}=\frac{k}{v_c}, \tag{48}$$

where k is a constant that depends on the control method used in the ICC defining its gain. Considering (9), then, substituting the power in terms of the input voltage and R_{LFR} while averaging the aforementioned equation, yields,

$$\frac{v_g^2}{R_{LFR}}=C_x v_o \frac{dv_o}{dt}+v_o i_{oX}. \tag{49}$$

Solving (10) and (48) into (49), and then perturbing the obtained equation, considering $i_{oX}=I_{oX}+\hat{i}_{oX}$, $v_c=V_c+\hat{v}_c$ and $v_g=V_g+\hat{v}_g$, while eliminating the second order and dc terms, yields,

$$\frac{V_{gp}^2}{2k}\hat{v}_g+\frac{V_g V_c}{k}\hat{v}_c=C_X\left(nV_{\gamma_{\_LED}}+I_{oX}nr_{LED}\right)nr_{LED}\frac{d\hat{i}_{oX}}{dt}+\left(nV_{\gamma_{\_LED}}+2I_{oX}nr_{LED}\right)\hat{i}_{oX}. \tag{50}$$

Note that lower case characters are used for the static analysis, capitalized characters are used for constant values and to particularize the equation in a determined point of operation, and lower case characters with a circumflex represent small ac variations. By applying the Laplace transform to (50), it becomes simple to solve for i_{oX} obtaining,

$$\hat{i}_{oX}=\frac{\frac{V_g V_c}{k}\hat{v}_g+\frac{V_g^2}{2k}\hat{v}_c}{C_X\left(nV_{\gamma_{\_LED}}+I_{oX}nr_{LED}\right)nr_{LED}s+\left(nV_{\gamma_{\_LED}}+2I_{oX}nr_{LED}\right)}. \tag{51}$$

Hence, from (51) the transfer function that relates $\hat{i}_{oX}$ to $\hat{v}_c$ and $\hat{i}_{oX}$ to $\hat{v}_b$ can be yielded for any of the cells described previously in the first scheme of control, depicted in Fig. 7 (a), as,

$$G_{i_{oX}v_c}(s)=\left.\frac{\hat{i}_{oX}}{\hat{v}_c}\right|_{\hat{v}_g=0}=\frac{\frac{V_g^2}{2k\left(nV_{\gamma_{\_LED}}+2I_{oX}nr_{LED}\right)}}{\frac{C_X\left(nV_{\gamma_{\_LED}}+I_{oX}nr_{LED}\right)nr_{LED}}{\left(nV_{\gamma_{\_LED}}+2I_{oX}nr_{LED}\right)}s+1}, \tag{52}$$

and,

$$G_{i_{oX}v_g}(s)=\left.\frac{\hat{i}_{oX}}{\hat{v}_g}\right|_{\hat{v}_c=0}=\frac{\frac{V_g V_c}{k\left(nV_{\gamma_{\_LED}}+2I_{oX}nr_{LED}\right)}}{\frac{C_X\left(nV_{\gamma_{\_LED}}+I_{oX}nr_{LED}\right)nr_{LED}}{\left(nV_{\gamma_{\_LED}}+2I_{oX}nr_{LED}\right)}s+1}. \tag{53}$$

In order to obtain the transfer function to be used for the second scheme of control, an extra step is required from the previous analysis to obtain the relationship between $\hat{i}_{oX}$ and $\hat{I}_o$. This requires the averaging and linearizing of (1), which yields,

$$I_o=\alpha(i_{oR}+i_{oS}+i_{oT}). \tag{54}$$

Then, (54) can be perturbed considering, $i_{oX}=I_{oX}+\hat{i}_{oX}$, yielding:

$$I_o=\alpha\left(I_{oR}+\hat{i}_{oR}+I_{oS}+\hat{i}_{oS}+I_{oT}+\hat{i}_{oT}\right). \tag{55}$$

At this point, the analysis takes into account for the sake of simplification that all phases are going to be perturbed at the same time. Then, removing the dc components and applying the Laplace transform, yields,

$$\hat{I}_o(s)=3\alpha\hat{i}_{oX}. \tag{56}$$

Finally, the combination of (53) and (54) with (55) give the transfer function for the second scheme of control, depicted in Fig. 7 (b), as follows,

This article has been accepted for publication in a future issue of this journal, but has not been fully edited. Content may change prior to final publication. Citation information: DOI 10.1109/JESTPE.2018.2868950, IEEE Journal of Emerging and Selected Topics in Power Electronics

TABLE I. SUMMARY OF V_c, $\hat{v}_c$ AND K FOR DIFFERENT COMMON DC-DC CONVERTERS.

	V_c	$\hat{v}_c$	k
Boost operating in CCM with MBC [27]	V_c	$\hat{v}_c$	G_1
Boost operating in BCM [28]	T_{on}	$\hat{t}_{on}$	$\frac{L}{2}$
Flyback operating in DCM [29]	D^2	$2D\hat{d}$	$\frac{2L}{T_s}$

$$G_{l_o v_c}(s) = \left.\frac{\hat{I}_o(s)}{\hat{v}_c(s)}\right|_{\hat{v}_g=0} = 3\alpha G_{i_{oX}v_c}(s). \quad (57)$$

and,

$$G_{l_o v_c}(s) = \left.\frac{\hat{I}_o(s)}{\hat{v}_g(s)}\right|_{\hat{v}_c=0} = 3\alpha G_{i_{oX}v_g}(s). \quad (58)$$

The analysis carried out in this section can be extrapolated to any dc-dc converter operating as an LFR. For this reason, Table I, summarizes the values that V_c, $\hat{v}_c$ and k should take for three different scenarios. It should be noted that the parameter G_1 introduced in Table I refers to the gain of the input current sensor of the boost PFC converter.

V. EXPERIMENTAL RESULTS

For the sake of validating the proposal of this work, which is to drive LEDs in three-phase power grids, a prototype has been built controlling three boost converters working in CCM with an MBC. The control of each cell is performed with the help of an analog IC, the UCC3817 widely used in PFC. In particular, the control methodology used by the experimental prototype is the one described in Fig. 7 (a). The LED driver is designed in such a way that each cell is required to drive two strings in parallel of 20 LEDs (L150-5770502400000), which are equivalent to 490 V at 100 W. The number of LEDs selected in series on a string is not done randomly and is picked ensuring that the sum of knee voltages from the LEDs in a string at the operating temperature is higher than the maximum input voltage in the worst case scenario of the power grid, which is around 400 V for the European power grid. This fact is based on the inherent behaviour of a boost converter, which is only able to increase the voltage at its input. Otherwise, the driver would not be able to guarantee full dimming operation.

The components that comprise each of the cells are summarized in Table II, where the boost inductance has been designed in accordance to the mathematical analysis carried out to study the limits between CCM and DCM in order to guarantee operation in CCM.

Fig. 8, shows a picture of the designed prototype with its three cells, its central control unit and the designed luminaire. The central control unit is responsible for two functionalities: the first one being the start-up of the LED driver, and the second, giving the command to each cell to provide the LEDs

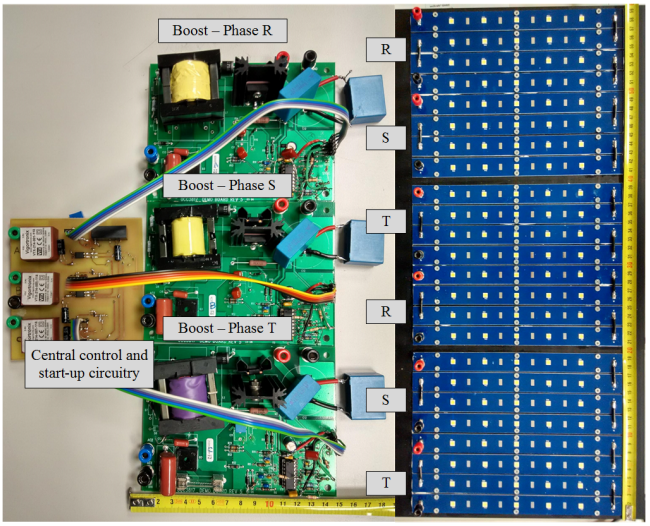

Fig. 8. Photograph of the experimental setup.

TABLE II. SUMMARY OF THE COMPONENTS USED IN EACH CELL

Fig. 2 reference	VALUE
L_1, L_2 and L_3	1.7 mH
Q_1, Q_2 and Q_3	IPW65R190C7
D_1, D_2 and D_3	IDH06SG60C
C_R, C_S and C_T	10 µF

with the same current. In terms of the start-up, it can be tackled in a similar fashion to [36], [37]. Following the same principle, the cells are off at the start of the LED driver until the output capacitors are all charged to the maximum voltage achievable in a star connection through the inrush current diode, at which point all the cells are started up. Hence, an isolated signal is given to the control unit of each cell to start-up the boost converter. In the picture, it can also be seen that the LED strings are distributed between phases in order to ensure a better blend of the light.

A. Output capacitor analysis

The first experimental analysis is carried out in order to validate the operation of one of the cells when it is connected to a single-phase power grid at its input and an LED string at its output with a high current ripple and voltage. The design of the cell has to be carried out following the traditional design criteria for a single-phase ac-dc LED driver (i.e., meeting the power requirements of the LED load, selection of semiconductor devices, etc.), while keeping in mind two significant changes: the selection of the output capacitance and the selection of the magnetic components and switching frequency. The selection of the output capacitance has to be done in accordance to (23), which marks a significant change to the traditional scenario. In addition, the selection of the magnetic components and switching frequency has to be done in accordance to the analysis carried out in Section III depending on the selected method used to ensure the LFR performance. It should also be noted that taking into account the modularity of the converter it is possible to optimize a cell

This article has been accepted for publication in a future issue of this journal, but has not been fully edited. Content may change prior to final publication. Citation information: DOI 10.1109/JESTPE.2018.2868950, IEEE Journal of Emerging and Selected Topics in Power Electronics

for a certain power and add as many cells as required for a high power ac-dc LED driver.

In that sense, Fig. 9 shows that the input current is adequately in phase with the input voltage ensuring, as expected, an LFR performance at the maximum output power of the cell (i.e. 100 W) while working in CCM. Particularly, Fig. 9 (a) depicts the high current ripple due to the use of a 10μF and the light output measured with a transimpedance amplifier (TSL-257), located at a fixed distance of 20cm, which supplies at its output a certain voltage, v_L, depending on the light falling upon the photodiode. In contrast, Fig. 9 (b) shows the voltage withstood by the LEDs for this scenario in which the lowest voltage never falls below the 400 V mark set before. However, this is the best-case scenario, as the lowest current is far from being zero to test whether the selection of LEDs is acceptable. In order to ensure an adequate performance in terms of its output voltage, Fig. 10 shows a snapshot of the oscilloscope when dimming the driver to an output power of 25 W. As can be seen, the output current reaches zero, and it is at this point where the minimum output voltage is reached being slightly higher than 400 V.

Although, the operation for an LED load has been validated, the analysis carried out in terms of the output capacitor has not. For that matter, Fig. 11 summarizes three different measurements of current across the LEDs performed at

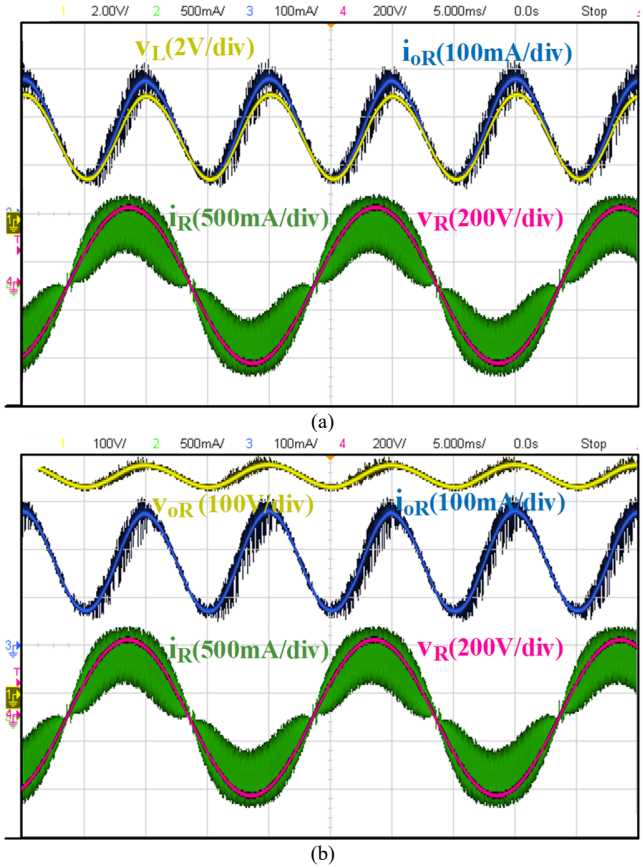

Fig. 9. Standalone operation of one the cells that comprise the LED driver at maximum power, depicting both input and output current, input voltage, and (a) light output measurement or (b) output voltage measurement.

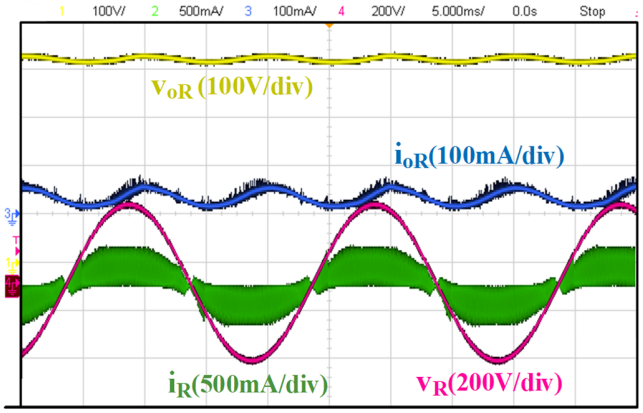

Fig. 10. Standalone operation of one the cells that comprise the LED driver at a quarter of the maximum output power.

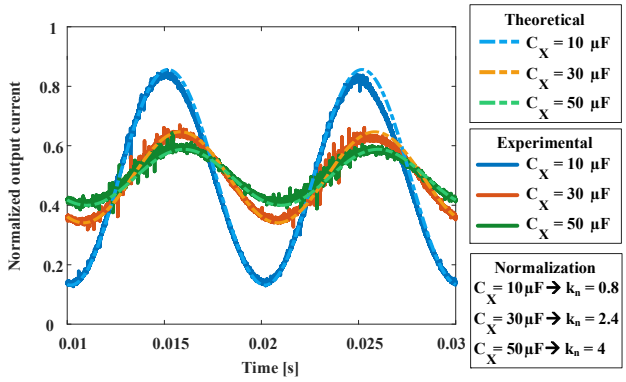

Fig. 11. Output current across the LEDs when varying the output capacitor of the cell.

maximum output power after being extracted from the oscilloscope, considering the only variable that changes in the cell is the value of the output capacitor. As can be seen, the higher the value of the output capacitor, the lower the current ripple. Furthermore, the obtained experimental results, shown in Fig. 11, are compared to the analytical model presented in Section II. In fact, with this comparison it can be seen, at a glance, that the developed model is extremely accurate.

B. Evaluation in a real three-phase power grid

After having validated the operation of the cells individually, the LED driver has been assembled and connected to the real three-phase power grid, by means of a three-wire connection. Under these conditions, the waveforms presented in Fig. 12 have been obtained from the oscilloscope at maximum load, i.e. 300 W. Particularly, Fig. 12 (a) depicts the input waveforms of the three-phase LED driver after the EMI filter, which is not included in the schematic of Fig. 2. As can be seen, phase R achieves an LFR performance. This performance can be assumed for the other two phases, considering the phase-shift between the currents. Moreover, Fig. 12 (b) shows the current across the LED strings for each of the cells presenting extremely similar current levels for all of them, although, there exists slight difference caused by the tolerances of the components that comprise each cell. Its sum, measured again with a photodiode connected to a

This article has been accepted for publication in a future issue of this journal, but has not been fully edited. Content may change prior to final publication. Citation information: DOI 10.1109/JESTPE.2018.2868950, IEEE Journal of Emerging and Selected Topics in Power Electronics

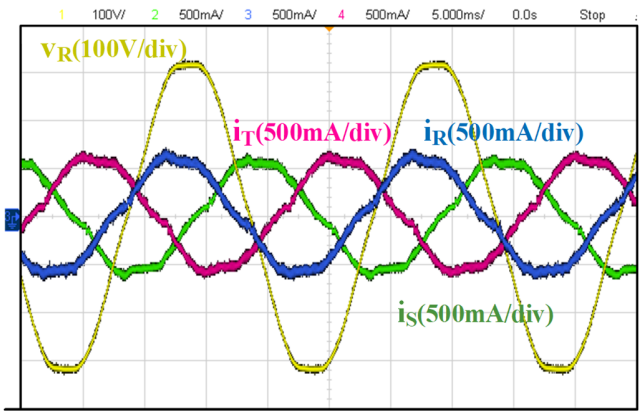

(a)

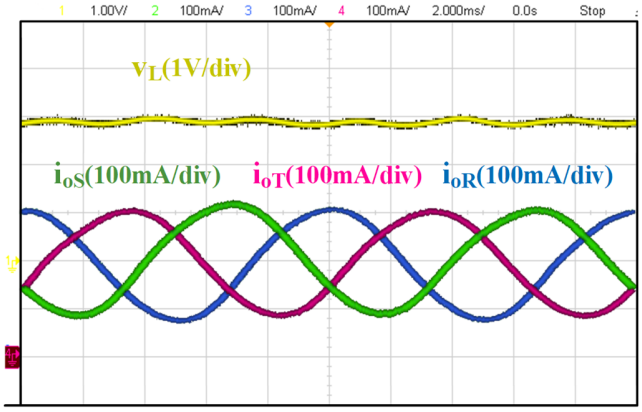

(b)

Fig. 12. Experimental waveforms at maximum load. (a) Input voltage and currents. (b) Output currents and light output.

transimpedance amplifier, in this case at a fixed distance of 60 cm, is comprised of a dc level with a low frequency ripple at 300 Hz and is almost not affected by this error. Considering the amplitude of this ripple the light output of the driver can be considered to be constant. In fact, Fig. 13 displays a snapshot showing the performance of the driver at 25 W, where it can also be seen the similarity between the output currents with an adequate phase-shift in between, and an almost constant light output.

The almost constant light output of the driver validates the analysis carried out. However, the low frequency ripple needs to be evaluated to ensure a flicker free performance. In that respect, the IEEE standard 1789-2015 will be used to limit the biological effects and detection of flicker in general illumination. In order to achieve this performance the modulation (%), normally referred as Mod. (%), should be kept withing the shaded region defined in [38] for all the harmonic components of the light output. Consequently, the Mod. (%) for each of the harmonics can be defined as follows,

$$\text{Mod.}(\%)(\text{m})=\frac{L_{H,max}(\text{m})-L_{H,min}(\text{m})}{L_{H,max}(\text{m})+L_{H,min}(\text{m})+L_{dc}}\cdot 100, \qquad (59)$$

where m defines t he number of the harmonic in reference to the fundamental one, L_{dc} represents the average luminance of the LED driver, and $L_{H,max}$ and $L_{H,min}$ correspond to the maximum and minimum luminance for harmonic m, respectively.

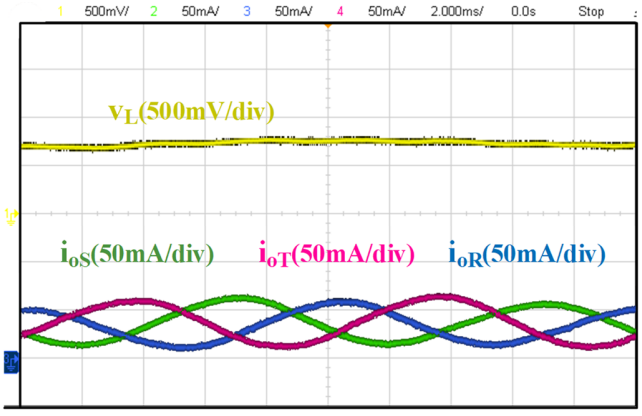

Fig. 13. Experimental output currents and light output waveforms at a quarter of the maximum output power.

The luminance over time of the LED driver has been obtained for a line period and has been processed with MATLAB in order to attain the harmonic components with the help of the Fourier series, considering the line frequency as the fundamental frequency. Fig. 14 shows that the Mod. (%) of all the harmonic components 50 Hz to 3 kHz fall under the shaded region which represents the recommended operating area from. A flicker free performance of the proposed LED driver can then be assured from this analysis.

C. Electrical performance

The proposal of summing the light output of each cell has been validated for the proposed LED driver. However, two characteristics need to be evaluated before closing the analysis. The first one is the compliance with the regulation IEC 61000-3-2, in which the input current harmonics at maximum power are compared with the limits set in the aforementioned regulation for each of the phases. Fig. 15 summarizes the results from this comparison assuring compliance with the regulation.

In that sense, a few parameters can be of interest from the point of view of the input current quality, as are the THD and

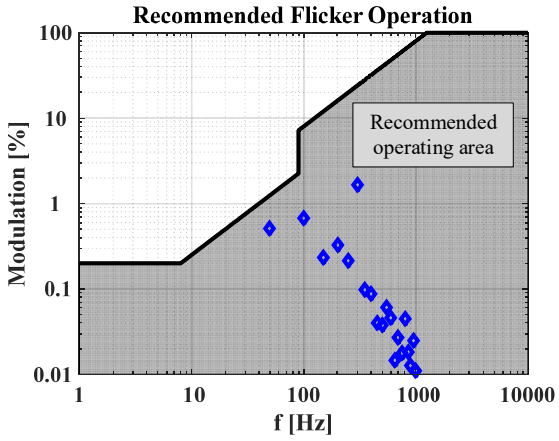

Fig. 14. Recommended flicker operation for the proposed LED driver [38].

This article has been accepted for publication in a future issue of this journal, but has not been fully edited. Content may change prior to final publication. Citation information: DOI 10.1109/JESTPE.2018.2868950, IEEE Journal of Emerging and Selected Topics in Power Electronics

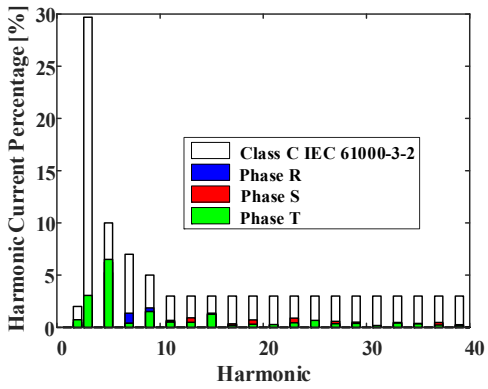

Fig. 15. Harmonic content of each phase for the proposed driver under study assuring compliance with Class C IEC 61000-3-2.

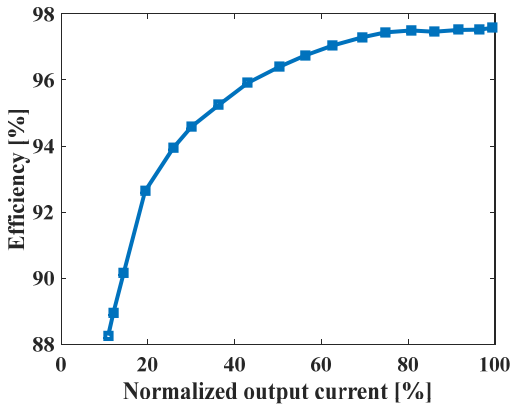

Fig. 16. Electrical efficiency measured under different dimming conditions at 400 Vrms.

TABLE III. SUMMARY OF THD, PF AND EFFICIENCY FOR DIFFERENT INPUT VOLTAGES

Phase/ Max. input voltage		R	S	T
380 Vrms	THD [%]	6.7	6.8	7
	PF	0.997	0.997	0.997
	Efficiency [%]		96.9	
400 Vrms	THD [%]	6.7	7.1	7.3
	PF	0.995	0.995	0.995
	Efficiency [%]		97.5	
420 Vrms	THD [%]	7.4	7.6	7.9
	PF	0.992	0.992	0.997
	Efficiency [%]		98.2	

PF. These parameters are summarized in Table III for three different input voltages with their respective efficiency at full load. As can be seen, the measured THD is about 7% and the PF is 0.99, furthermore, the LED driver presents an efficiency of 96.9% for the lowest input voltage and 98.2% for its maximum.

The efficiency has been measured under different dimming conditions at 400 Vrms, as shown in Fig. 16, obtaining a maximum efficiency of 97.5% at full load, which is equivalent to 42.000 lm, outputting a luminous efficacy of 140 lm/W. It should be noted that, even if the minimum output current shown in Fig. 16 is equivalent to 25 W, the driver is able to achieve full dimming conditions with an output power that almost reaches zero.

As regards the efficiency measurements, the input power can be easily obtained, however, the output power becomes more complicated as it is comprised of a dc component and an ac component. For this reason, the instantaneous value of the power consumed by each LED load has been measured during several times the line period. Then, this waveform has been averaged within the same time in order to attain the power consumed by each LED load. After having all the average values, they have summed in order to obtain the total power consumption, which is then compared with the total input power at certain operating point set by the current reference.

Finally, a comparison of the proposed ac-dc LED driver has been made with state-of-the-art three-phase ac-dc LED drivers, in terms of efficiency, number of components, percent flicker, etc. This comparison is shown in Table IV, and as can be seen, the proposed ac-dc LED driver is able to achieve an efficiency 5.5 points higher than the closest state of the art solution with a very low percent flicker, low output capacitance and low component count. In fact, the value of the output capacitance can be lowered even further at the cost of increasing the output current ripple on the LEDs without having an actual impact on the percent flicker. It should also be noted that being the proposed ac-dc LED driver a modular solution, it is also easy to scale its power to the requirements of the design by including more modules, if required.

VI. CONCLUSIONS

The presented modular three-phase ac-dc LED driver removes the electrolytic capacitor and the second stage aiming for LED driving of high power luminaires that require a long lifespan, generally in inaccessible places. In addition, the proposed solution complies with the most restrictive harmonic regulation and ENERGY STAR®. The presented idea is based on taking advantage of the light properties to sum the light output of each phase, thus not requiring the connection of the output of each cell in parallel to remove the electrolytic capacitor. It is thanks to this fact that galvanic isolation can be removed being able to use a single-stage approach per cell.

In order to remove the electrolytic capacitor from the PFC converters that comprise each cell, high current ripples are allowed across the LED loads. However, this high ripple may end up requiring the oversizing of the LED loads. It is this fact that leads to the theoretical study in terms of the output capacitance to check the feasibility of having a small sized capacitor that ensures flicker free and a gentler ripple on the LEDs. The proposed model is validated showing a high accuracy with an error below 5%, which helps in order to achieve an optimum design. In addition, due to this high ripple the limits between CCM and DCM had to be revaluated, yielding a handful of equations that are key for the design of the proposed ac-dc LED driver.

The experimental results have shown that the proposed LED driver is capable of achieving a constant light

This article has been accepted for publication in a future issue of this journal, but has not been fully edited. Content may change prior to final publication. Citation information: DOI 10.1109/JESTPE.2018.2868950, IEEE Journal of Emerging and Selected Topics in Power Electronics

TABLE IV. COMPARISON OF STATE OF THE ART THREE-PHASE AC-DC LED DRIVERS.

		REFERENCES			
	Proposed	[13]	Delco ac-dc LED driver [15]	Multi-cell ac-dc LED driver [15], [17]	[22]
Output Power [W]	300	54	100	100	216
Efficiency [%]	97.5	77	90.7	91.2	92
THD [%]	7	6.72	8	8	4.22
Switching frequency [kHz]	100	40	100	100	25-50
Output capacitor [µF]	10	-	10	10	80
Output voltage [V]	480	40	48	48	125
Percent flicker at six times the mains frequency	2	-	15	15	4.97
Modular	Yes	No	Yes	Yes	No
Galvanic isolation	No	Yes	Yes	Yes	No
Number of MOSFETs	3	1	3	6	6
Number of high frequency diodes	3	3	3	6	7
Number of transformers	0	3	3	6	0
Number of inductances	3	2	-	-	4

output meeting the flicker recommendation, compliance with the harmonic injection regulation and a high efficiency. In fact, the efficiency increase compared to three-phase state of the art LED drivers is not inconsequential, improving those solutions by more than 5.5% efficiency [13], [15], [17], [22]. Furthermore, the discussed control methods for the proposal are not more complex or costly than other modular solutions, becoming a possibility the input parallelization of several cells per phase, to further increase the power capabilities of the driver, without increasing or changing the central unit. In fact, taking advantage of the independency of the cells, when several cells are used per phase, if a failure occurs it is possible for the central control unit to switch off an equivalent amount of cells on the other phases at the cost of reducing the maximum power of the solution. For the aforementioned reasons, this driver is an ambitious solution to drive LEDs in three-phase power grid when galvanic isolation is not required.

REFERENCES

[1] M. Arias, A. Vazquez, and J. Sebastian, "An overview of the AC-DC and DC-DC converters for LED lighting applications," Automatika—J. Control, Measure., Electr., Comput. Commun., vol. 53, pp. 156–172, 2012.

[2] ENERGY STAR® Program Requirements Product Specification for Lamps (Light Bulbs) – Elegibility Criteria, V. 2.0, Oct. 2016.

[3] ENERGY STAR® Program Requirements Product Specification for Luminaires (Light Fixtures) – Elegibility Criteria, V. 2.0, Jan. 2016.

[4] Electromagnetic compatibility (EMC) – Part 3-2: Limits – Limits for harmonic current emissions (equipment input current < 16 A per phase), document IEC 61000-3-2, 2014.

[5] Q. Hu and R. Zane, "Minimizing Required Energy Storage in Off-Line LED Drivers Based on Series-Input Converter Modules," in IEEE Transactions on Power Electronics, vol. 26, no. 10, pp. 2887-2895, Oct. 2011.

[6] J. He, X. Ruan and L. Zhang, "Adaptive Voltage Control for Bidirectional Converter in Flicker-Free Electrolytic Capacitor-Less AC–DC LED Driver," in IEEE Transactions on Industrial Electronics, vol. 64, no. 1, pp. 320-324, Jan. 2017.

[7] D. Camponogara, D. R. Vargas, M. A. Dalla Costa, J. M. Alonso, J. Garcia and T. Marchesan, "Capacitance Reduction With An Optimized Converter Connection Applied to LED Drivers," in IEEE Transactions on Industrial Electronics, vol. 62, no. 1, pp. 184-192, Jan. 2015.

[8] Y. Qiu, L. Wang, H. Wang, Y. F. Liu and P. C. Sen, "Bipolar Ripple Cancellation Method to Achieve Single-Stage Electrolytic-Capacitor-Less High-Power LED Driver," in IEEE Journal of Emerging and Selected Topics in Power Electronics, vol. 3, no. 3, pp. 698-713, Sept. 2015.

[9] Y. Wang, Y. Guan, J. Huang, W. Wang and D. Xu, "A Single-Stage LED Driver Based on Interleaved Buck–Boost Circuit and LLC Resonant Converter," in IEEE Journal of Emerging and Selected Topics in Power Electronics, vol. 3, no. 3, pp. 732-741, Sept. 2015.

[10] J. C. W. Lam and P. K. Jain, "Isolated AC/DC Offline High Power Factor Single-Switch LED Drivers Without Electrolytic Capacitors," in IEEE Journal of Emerging and Selected Topics in Power Electronics, vol. 3, no. 3, pp. 679-690, Sept. 2015.

[11] J. W. Kolar, H. Ertl and F. C. Zach, "A novel three-phase single-switch discontinuous-mode AC-DC buck-boost converter with high-quality input current waveforms and isolated output," in IEEE Transactions on Power Electronics, vol. 9, no. 2, pp. 160-172, Mar 1994.

[12] J. Minbock and J. W. Kolar, "Design and experimental investigation of a single-switch three-phase flyback-derived power factor corrector," INTELEC. Twenty-Second International Telecommunications Energy Conference (Cat. No.00CH37131), Phoenix, AZ, 2000, pp. 471-478.

[13] M. R. Mendonça, E. Mineiro; Sá, R. P. Coutinho and F. L. M. Antunes, "AC-DC single-switch three-phase converter with peak current control for power LEDs," Industry Applications (INDUSCON), 2014 11th IEEE/IAS International Conference on, Juiz de Fora, 2014, pp. 1-6.

[14] R. F. Brewster and A. H. Barret, "Three Phase AC to DC voltage converter with Power Line Harmonic Current Reduction", U.S. patent 4 143 414, March 6, 1979.

[15] I. Castro, D. G. Lamar, M. Arias; M. M. Hernando, J. Sebastian, "Multi-cell three phase ac-dc driver for HB-LED lighting applications," in IEEE Transactions on Industry Applications, vol.PP, no.99, pp.1-1.

[16] J. Sebastián, I. Castro, D. G. Lamar, A. Vázquez and K. Martín, "High power factor modular polyphase AC/DC converters with galvanic isolation based on Resistor Emulators," 2016 IEEE Applied Power Electronics Conference and Exposition (APEC), Long Beach, CA, 2016, pp. 25-32.

[17] I. Castro, D. G. Lamar, M. Arias, J. Sebastian and M. M. Hernando, "Three phase converter with galvanic isolation based on loss-free resistors for HB-LED lighting applications," 2016 IEEE Applied Power Electronics Conference and Exposition (APEC), Long Beach, CA, 2016.

[18] M. Arias, D. G. Lamar, J. Sebastian, D. Balocco and A. A. Diallo, "High-Efficiency LED Driver Without Electrolytic Capacitor for Street Lighting," in IEEE Transactions on Industry Applications, vol. 49, no. 1, pp. 127-137, Jan.-Feb. 2013.

[19] X. Wu, J. Zhang and Z. Qian, "A Simple Two-Channel LED Driver With Automatic Precise Current Sharing," in IEEE Transactions on Industrial Electronics, vol. 58, no. 10, pp. 4783-4788, Oct. 2011.

[20] M. Arias, M. Fernández Diaz, D. G. Lamar, D. Balocco, A. Aguissa Diallo and J. Sebastián, "High-Efficiency Asymmetrical Half-Bridge Converter Without Electrolytic Capacitor for Low-Output-Voltage AC–DC LED Drivers," in IEEE Transactions on Power Electronics, vol. 28, no. 5, pp. 2539-2550, May 2013.

[21] M. Arias, I. Castro, D. G. Lamar, A. Vázquez and J. Sebastián, "Optimized design of a high input-voltage-ripple-rejection converter for LED lighting," in IEEE Transactions on Power Electronics, vol. PP, no. 99, pp. 1-1.

[22] R. P. Coutinho, K. C. A. de Souza, F. L. M. Antunes and E. Mineiro Sá, "Three-Phase Resonant Switched Capacitor LED Driver With Low Flicker," in IEEE Transactions on Industrial Electronics, vol. 64, no. 7, pp. 5828-5837, July 2017.

[23] C. S. Wong, K. H. Loo, Y. M. Lai, M. H. L. Chow and C. K. Tse, "An Alternative Approach to LED Driver Design Based on High-Voltage Driving," in IEEE Transactions on Power Electronics, vol. 31, no. 3, pp. 2465-2475, March 2016.

[24] N. Pousset, B. Rougie, and A. Razet, "Impact of current supply on LED colour," Lighting Res. Technol., vol. 42, no.4, pp. 371–383, August 2010.

[25] W. Feng, Y. He and F. G. Shi, "Investigation of LED Light Output Performance Characteristics Under Different Alternating Current Regulation Modes," in IEEE Journal of Selected Topics in Quantum Electronics, vol. 17, no. 3, pp. 720-723, May-June 2011.

[26] H. Sun, "Sports Lighting – Design Considerations For The Beijing 2008 Olympic Games", GE Beijing 2008 Olympic Games Solutions, 2008.

[27] L. H. Dixon, "High power factor preregulators for off-line power supplies", Unitrode Power Supply Design Seminar, 1988, pp. 6.1-6.16.

[28] L. Rossetto, G. Spiazzi, and P. Tenti, "Control techniques for power factor correction converters, " in Proc. Int. Conf. Power Electron. Motion Control, Warsaw, Poland, 1994, pp. 1310–1318.

[29] Erickson, M. Madigan and S. Singer, "Design of a simple high-power-factor rectifier based on the flyback converter," Fifth Annual Proceedings on Applied Power Electronics Conference and Exposition, Los Angeles, CA, USA, 1990, pp. 792-801.

[30] T. Freegarde. Introduction to the Physics of Waves. Cambridge University Press, 2012.

[31] J. Sebastian, J. A. Cobos, J. M. Lopera and U. Uceda, "The determination of the boundaries between continuous and discontinuous conduction modes in PWM DC-to-DC converters used as power factor preregulators," in IEEE Transactions on Power Electronics, vol. 10, no. 5, pp. 574-582, Sep 1995.

[32] K. M. Smedley and S. Cuk, "One-cycle control of switching converters," in IEEE Transactions on Power Electronics, vol. 10, no. 6, pp. 625-633, Nov 1995.

[33] J. Sebastian, D. Gonzalez Lamar, M. Arias Perez de Azpeitia, M. Rodriguez and A. Fernandez, "The Voltage-Controlled Compensation Ramp: A Waveshaping Technique for Power Factor Correctors," in IEEE Transactions on Industry Applications, vol. 45, no. 3, pp. 1016-1027, May-june 2009.

[34] K. Yao, X. Ruan, X. Mao and Z. Ye, "Reducing Storage Capacitor of a DCM Boost PFC Converter," in IEEE Transactions on Power Electronics, vol. 27, no. 1, pp. 151-160, Jan. 2012.

[35] S. Singer and A. Fuchs, "Multiphase AC-DC conversion by means of loss-free resistive networks," in IEE Proceedings - Circuits, Devices and Systems, vol. 143, no. 4, pp. 233-240, Aug 1996.

[36] L. Huber, M. Kumar and M. M. Jovanovic, "Analysis, design, and evaluation of three-phase three-wire isolated ac-dc converter implemented with three single-phase converter modules," 2016 IEEE Applied Power Electronics Conference and Exposition (APEC), Long Beach, CA, 2016, pp. 38-45.

[37] M. Kumar, L. Huber and M. M. Jovanovic, "Startup procedure for three-phase three-wire isolated ac-dc converter implemented with three single-phase converter modules," 2016 IEEE Applied Power Electronics Conference and Exposition (APEC), Long Beach, CA, 2016, pp. 46-53.

[38] IEEE Recommended Practices for Modulating Current in High-Brightness LEDs for Mitigating Health Risks to Viewers," in IEEE Std 1789-2015 , vol., no., pp.1-80, June 5 2015.

Ignacio Castro (S'14, M'18) was born in Gijón, Spain, in 1989. He received the M.Sc. degree in telecommunication engineering and the Ph.D. in electrical engineering from the University of Oviedo, Gijón, Spain, in 2014 and 2018, respectively.

From 2014 to 2018, he has been a research assistant and member of the power supply group in the University of Oviedo. In August 2018, he joined United Technologies Research Centre in Ireland as a Senior Research Engineer.

His research interests include low and medium power dc–dc converters, modeling, simulation and control of dc-dc converters and power-factor correction ac–dc converters.

Aitor Vazquez (S'2010, M'2015) was born in Oviedo, Spain, in 1984. He received the M.Sc. degree in telecommunication engineering, in 2009, and the PhD. degree in electrical engineering in 2016, from the University of Oviedo, Gijon, Spain. He became a Member of the Power Supply System Group, University of Oviedo, in 2010. His current research interests include modularization techniques applied to bidirectional dc–dc converters for HEV, battery management power supplies, DC distribution grids, powerfactor corrector ac–dc converters and energy recovery systems.

Manuel Arias (s'05 M'10) received the M. Sc. degree in electrical engineering from the University of Oviedo, Spain, in 2005 and the Ph. D. degree from the same university in 2010. In 2007 he joined the University of Oviedo as an Assistant Professor and since 2016 he is an Associate Professor at the same university. His research interests include ac-dc and dc-dc power converters, battery-cell equalizers and LED lighting.

Diego G. Lamar (M'08) was born in Zaragoza, Spain, in 1974. He received the M.Sc. degree, and the Ph.D. degree in Electrical Engineering from the University of Oviedo, Spain, in 2003 and 2008, respectively. In 2003 and 2005 he became a Research Engineer and an Assistant Professor respectively at the University of Oviedo. Since September 2011, he has been an Associate Professor. His research interests are focused in switching-mode power supplies, converter modelling, and power-factor-correction converters.

Marta M. Hernando (M'95-SM'11) was born in Gijón, Spain, in 1964. She received the M.Sc. and Ph.D. degrees in Electrical Engineering from the University of Oviedo, Gijón, Spain, in 1988 and 1992, respectively. She is currently a Professor at the University of Oviedo. Her main research interests include switching-mode power supplies and high-power factor rectifiers.

Javier Sebastián (M'87-SM'11) was born in Madrid, Spain, in 1958. He received the M.Sc. degree from the Technical University of Madrid (UPM), and the Ph.D. degree in electrical engineering from the University of Oviedo, Spain, in 1981 and 1985, respectively. He was an Assistant Professor and an Associate Professor at both the UPM and the University of Oviedo. Since 1992, he has been with the University of Oviedo, where he is currently a Professor. His research interests are switching-mode power supplies, modeling of dc-to-dc converters, low output voltage dc-to-dc converters, high power factor rectifiers, LED drivers, dc-to-dc converters for envelope tracking techniques and the use of wide band-gap semiconductors in power supplies.